energies

MDPI

Article

Assessment of an Exhaust Thermoelectric Generator Incorporating Thermal Control Applied to a Heavy Duty Vehicle

Carolina Clasen Sousa [1,*], Jorge Martins [1], Óscar Carvalho [2], Miguel Coelho [2], Ana Sofia Moita [3] and Francisco P. Brito [1,4,*]

[1] MEtRICs, Mechanical Engineering Department, Campus of Azurem, University of Minho, 4800-058 Guimaraes, Portugal; jmartins@dem.uminho.pt
[2] CMEMS, Mechanical Engineering Department, Campus of Azurem, University of Minho, 4800-058 Guimaraes, Portugal; oscar.carvalho@dem.uminho.pt (Ó.C.); a74190@alunos.uminho.pt (M.C.)
[3] Instituto Universitário Militar—CINAMIL, Academia Militar, IN+ University of Lisbon, 1649-004 Lisboa, Portugal; moita.asoh@exercito.pt
[4] TEMA, Mechanical Engineering Department, Campus of Santiago, University of Aveiro, 3810-193 Aveiro, Portugal
* Correspondence: a78187@alunos.uminho.pt (C.C.S.); francisco@dem.uminho.pt (F.P.B.)

Abstract: The road transport industry faces the need to develop its fleet for lower energy consumption, pollutants and CO_2 emissions. Waste heat recovery systems with Thermoelectric Generators (TEGs) can directly convert the exhaust heat into electric energy, aiding the electrical needs of the vehicle, thus reducing its dependency on fuel energy. The present work assesses the optimisation and evaluation of a temperature-controlled thermoelectric generator (TCTG) concept to be used in a commercial heavy-duty vehicle (HDV). The system consists of a heat exchanger with wavy fins (WFs) embedded in an aluminium matrix along with vapour chambers (VCs), machined directly into the matrix, that grant the thermal control based on the spreading of local excess heat by phase change, as proposed by the authors in previous publications and patents. The TCTG concept behaviour was analysed under realistic driving conditions. An HDV with a 16 L Diesel engine was simulated in AVL Cruise to obtain the exhaust gas temperature and mass flow rate for each point of two cycle runs. A model proposed in previous publications was adapted to the new fin geometry and vapour chamber configuration and used the AVL Cruise data as input. It was possible to predict the thermal and thermoelectric performance of the TCTG along the corresponding driving cycles. The developed system proved to have a good capacity for applications with highly variable thermal loads since it was able to uncouple the maximisation of heat absorption from the regulation of the thermal level at the hot face of the TEG modules, avoiding both thermal dilution and overheating. This was achieved by the controlled phase change temperature of the heat spreader, that would ensure the spreading of the excess heat from overheated to underheated areas of the generator instead of wasting excess heat. A maximum average electrical production of 2.4 kW was predicted, which resulted in fuel savings of about 2% and CO_2 emissions reduction of around 37 g/km.

Keywords: heavy-duty vehicles; fuel efficiency; waste heat recovery; onboard electricity production; thermoelectric generators; thermal control; variable conductance heat pipes; vapour chambers

Citation: Sousa, C.C.; Martins, J.; Carvalho, Ó.; Coelho, M.; Moita, A.S.; Brito, F.P. Assessment of an Exhaust Thermoelectric Generator Incorporating Thermal Control Applied to a Heavy Duty Vehicle. *Energies* **2022**, *15*, 4787. https://doi.org/10.3390/en15134787

Academic Editor: Pedro J. Coelho

Received: 13 May 2022
Accepted: 20 June 2022
Published: 29 June 2022

1. Introduction

Within the increasing demand of the transport sector comes the challenge of reducing its fossil fuel consumption and emissions. According to the European scenario, it is expected that the passenger transport sector will increase by 40% and freight transport by 60% from 2010 to 2050. Being a sector which plays an important role in the European economy that still relies heavily on fossil fuels, the European Union has set several targets to control CO_2

emissions. For heavy transportation, CO_2 emissions must be reduced up to 30% by 2030, with an interim target of 15% in 2025 [1].

Combustion engines have numerous constraints that result in the dissipation of fuel energy, jeopardising their efficiency. In HDVs about 34% of the fuel energy is used to move the vehicle, while 30% is lost through exhaust gases, mainly in the form of thermal energy [2]. It is possible to conclude that instead of the major percentage of thermal losses being dissipated into the environment, it can be used as an energy source.

The thermal energy dissipated by the exhaust system can be reused through waste energy recovery systems, instead of being dissipated into the environment. Amongst the various waste energy conversion systems, those based on TEGs—Thermoelectric Generators—have a strong potential to be used if their current limitations are overcome. In fact, TEGs can convert thermal energy directly into electrical energy by the Seebeck principle. These are highly reliable devices, if carefully projected, have no moving parts, are small, require low maintenance, and can raise fuel efficiency up to 5%. Recent notable examples of this are the analysis, backed by experimental validation performed by Heber et al [3] which claimed the viability of TEGs in natural gas powered Heavy duty vehicles, with a fuel economy up to 2.8%, powers reaching 3 kW and an estimated amortization period of significantly less than 2 years. TEGs include several connected semiconductors, positively doped (p-type) and negatively doped (n-type), which create thermoelectric junctions, the p-n couples. As a temperature gradient is created across the thermoelectric junctions an electromotive force is induced, enabling, by implementing an electrical load, the flow of electrical current to the vehicle. However, TEGs have limitations regarding the maximum tolerated temperature and the sensitivity of their output to the thermal level. On the one hand, most commercially available TEGs can support only modest temperatures, typically 250 °C. On the other hand, to operate at their maximum efficiency, they need to be as close as possible to their maximum allowable temperature. This makes their optimisation under realistic driving conditions nearly impossible unless some thermal control may be implemented [4,5].

Thus, to fully exploit the TEGs efficiency, they should operate at uniform temperature and closest to their temperature limit. The heat exchanger must be capable of maximising the heat absorption as much as possible, independently of the driving cycle, which can have high or low exhaust temperatures, while ensuring that the temperature reaching the modules does not exceed its limit. Besides exploring new promising and affordable thermoelectric materials [6,7] The authors have been exploring a clever system to do this in a passive way, with a TCTG concept using either variable conductance thermosiphons (VCTS) [8–12] or Heat Pipes (HPs) [13]. In the former case, the phase change process was used to absorb and transfer all the exhaust heat to the TCTG. In the more recent developments, the phase change process was only used to spread the excess heat from hotter to cooler regions of the generator to overcome the above-mentioned problems through thermal control. This temperature control is achieved through the concept, proposed by the researchers, of heat spreading through a phase change. This consists of using a liquid/vapour phase change system embedded along the heat exchanger which has the role of absorbing the excess heat from overheated regions, keeping them below the maximum allowable temperature, and then spreading and delivering this heat to under-heated regions of the heat exchanger, optimising temperature levels in this region. The phase change temperature is regulated by adjusting the pressure of a non-condensable gas (NCG) that is pre-charged into the system and stabilises the saturation conditions. The heat exchanger prototypes referred in the previous studies incorporated stainless steel corrugated pipes for the exhaust flow within the generator. They would be embedded in a cast-aluminium matrix along with variable conductance heat pipes (VCHPs). The hot faces of the TEGs would be attached to the aluminium block, receiving the exhaust heat with the temperature already downgraded to the optimal level. The cold face of the TEG modules was attached to finned liquid-cooled plates. The VCHPs were responsible for the heat spreading effect explained above. They enabled the control of the temperature of the

hot faces of the TEGs, working as capillary-driven heat carriers/spreaders. In the VCHPs, the exhaust heat is absorbed at the evaporator section, generating vapour. This vapour will fill a lower or a higher fraction of the VCHP depending of the incoming thermal load at the exhaust. Vapour then carries the thermal energy to the condensation region where the heat is released to the TEGs by condensation. The condensates then return to the evaporator through the wick structure by the action of capillary pumping. Since the exhaust gas temperature is not constant, and the modules require uniform temperature, there is the need for a uniform phase change temperature inside the HPs irrespective of thermal load. This can only be obtained through variable conductance, which is implemented by filling part of the condenser with a non-condensable gas. This way, the vapour will fill a higher or lower portion depending on the available thermal energy, thus only a part of the condenser will be active and the rest, filled with the non-condensable gas, inactive. In the case of high exhaust temperatures, the heat transfer area in contact with the TEGs will be higher compared with lower exhaust temperature [13].

Corrugated pipes embedded in aluminium have issues regarding their minimum spacing in the casting process, reducing the compactness factor and consequently the heat transfer effectiveness. Moreover, VCHPs tend to be expensive, made of copper, a poor pressure-resistant material, and prone to corrosion in casting. Thus, an alternative approach to the aforementioned heat exchanger concept is, firstly, to replace the corrugated pipes with wavy fins (Wfs), notable due to their simplicity of manufacture and potential for thermal performance at a reasonably low-pressure drop. Additionally, another good alternative seems to be to replace the VCHPs by variable conductance vapour chambers (VCVCs), which have the same operation as VCHPs, but geometrically more compact, as they are flat, and can directly be machined into the cast aluminium matrix. Additionally, the VCs envisioned display enhanced surfaces which are laser textured to maximise heat transfer performance and provide capillary pumping. These surfaces are currently being developed under a project. This technique, could be more cost-effective, improve compactness of the system, customisation, and phase change performance [14,15].

There seems to be a notable potential for applying this system to HDVs since these vehicles will rely upon combustion engines for a longer time than light duty vehicles and additionally have driving cycles with very high average thermal loads. Thus, the present study assesses the potential of such a system. An HVD with a 12 L Diesel engine was simulated in AVL Cruise to extract the exhaust gas temperature and exhaust mass flow rate along the two driving cycles, the WHVC and Long Haul cycle run. Additionally, to observe the influence of the payload weight in the HDV, the simulation runs were performed with different HDV curb weight loads: full with 25 t, half with 12.75 t and empty with 7.5 t in the WHVC and the Long Haul cycle run, one simulation was performed with the truck on its full weight load, 25.5 t.

2. Heat Exchanger Concept

The proposed TCTG represented in Figure 1 consists of a heat exchanger that absorbs the exhaust heat through WF embedded in cast aluminium. Then, it transfers this heat by conduction across the aluminium to the TEGs that are attached to the aluminium block surface. A part of the heat absorbed by the modules is converted into electricity, while the rest of the heat crosses the TEG modules by conduction and is dissipated to the heat sinks, the CP, attached to the modules cold faces. The system can spread the heat from overheated regions of the heat exchanger to underheated regions avoiding excess temperature and providing heat flux uniformity due to the implementation of VCs. When the temperature is below the maximum, these VCs are inactive and all the heat is transferred by conduction across the heat exchanger. Once the maximum allowable operating temperature is overcome at the upstream regions of the heat exchanger, the working fluid that is contained inside the VCs starts boiling, absorbing the heat and preventing a further temperature rise at the overheated regions. The vapour thus generated condenses and releases the heat at the

cooler downstream regions of the heat exchanger providing optimal temperature level to all the regions of the heat exchanger reached by the vapour.

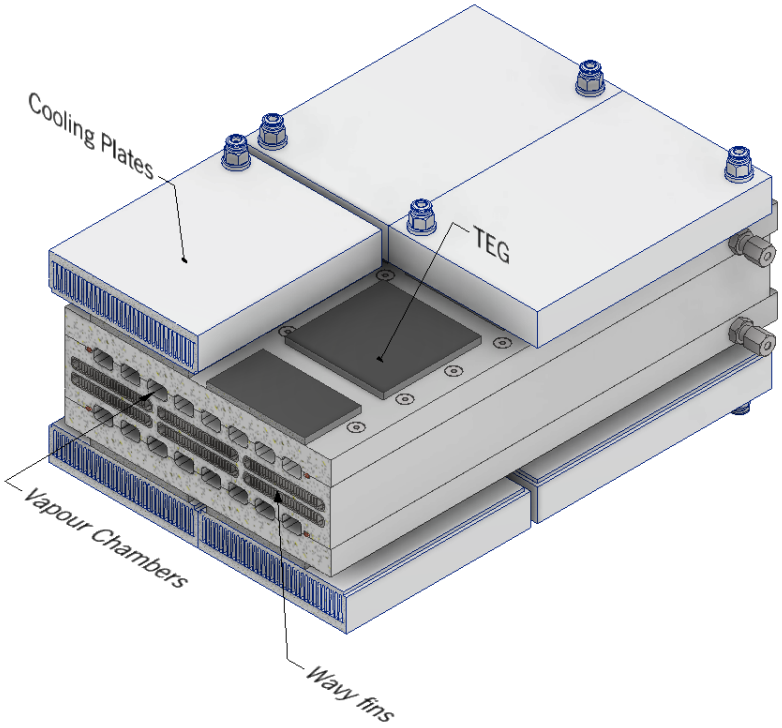

Figure 1. Scheme of the proposed heat exchanger for TCTG system.

2.1. Wavy Fins

WFs are compact heat exchangers of interest due to their great area density and geometry, which enhances the heat transfer effectiveness. The wavy pattern surface expands not only the length of the airflow path, but also the surface area, increasing the area density. In the system, WFs similar to the ones presented in Figure 2, produced by BorgWarner, were introduced [14,16]. WFs geometrical parameters are important for the system operation and are presented in the following sections. Figure 2 illustrates the considered geometrical characteristics.

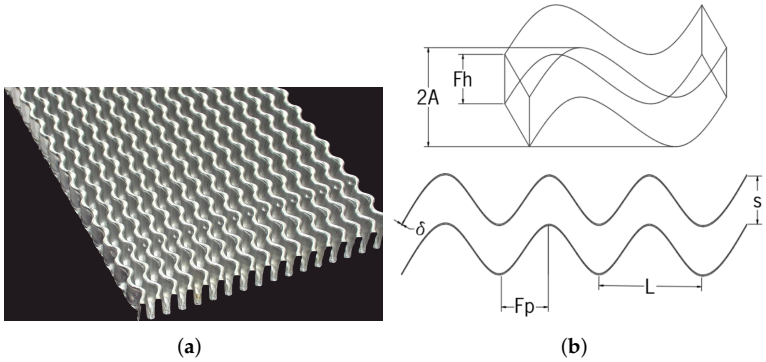

(**a**) (**b**)

Figure 2. Compact heat exchanger: (**a**) WFs image [17]. (**b**) Wavy fin geometry parameters: Fin pitch (Fp); fin high (Fh); fin spacing (s); fin thickness (δ); fin wavelength (L); twice the amplitude (2A).

Wavy Fins Empirical Correlations for Thermal Analysis

WFs require empirical correlations to allow the calculation of the heat transfer coefficient (h). The maximum air velocity in the fin (u_i) is an important design parameter and is obtained by Equation (1), where $\dot{v}$ is the gas volume flow and A_c the section area of the

fin channels. The hydraulic diameter of the fin entrance ($De = 4sF_h/2(s + F_h)$) and the air viscosity v are also used for Equation (2).

$$u_i = \frac{\dot{v}}{A_c} \tag{1}$$

$$Re = \frac{u_i \times De}{\mu} \tag{2}$$

The heat transfer and pressure drop characteristics for different geometry parameters, such as WF, can be reported in terms of the j factor and f, as a function of Re, where L_d is the wavy fin length:

$$j = 0.0836Re^{-0.2309}\left(\frac{F_p}{F_h}\right)^{0.1284}\left(\frac{F_p}{2A}\right)^{-0.153}\left(\frac{L_d}{L}\right)^{-0.326} \tag{3}$$

$$f = 1.16Re^{-0.309}\left(\frac{F_p}{F_h}\right)^{0.3703}\left(\frac{F_p}{2A}\right)^{-0.25}\left(\frac{L_d}{L}\right)^{-0.1152} \tag{4}$$

Dong Junqi [16] performed its analysis on WF by using a general CHE equation for the friction factor (f), where the constants kc and ke were graphically obtained according to the geometry parameters, hence the kc and ke are 0.4 and 0.2 in Equation (5), where A_o is the total air side heat transfer surface area.

$$f = \left(\frac{A_c}{A_o}\right)\left(\frac{2\Delta p}{\rho u^2} - kc - ke\right) \tag{5}$$

The surface effectiveness (η_a) and fin efficiency (η_{WF}) for the of wavy fins are determined by:

$$\eta_a = 1 - \frac{A_f}{A_o}(1 - \eta_f) \tag{6}$$

$$\eta_{WF} = \frac{tanh(m'l')}{m'l'}; m' = \sqrt{\frac{2h}{k_f\delta}}; l' = \frac{Fh}{2} \tag{7}$$

where A_f is the total finned area of the WF, k_f the thermal conductivity of the fin material.

2.2. Thermoeletric Modules

The thermoelectric generators considered were fairly standard Bismuth telluride modules and not particularly performing, as the main objective of the study was to assess the TCTG concept and not so much the specific output of the thermoelectric materials used. They were the GM250-127-28-10 from Adaptive Power Management ([18]). Their maximum operating temperature was 250 °C at the hot face. The geometrical and thermoeletric features are presented in Table 1.

Table 1. Parameters for hot side temp 250 °C and cold side temp 30 °C—adapted from [18].

Matched load output power	28.3 W
Matched load resistance	0.42 Ω ± 15%
Open circuit voltage	6.9 V
Matched load output	8.2 A
Matched load output voltage	3.45 V
Heat flow through module	~566 W
Maximum compress (non-destructive)	1 MPa
Maximum operation temperature	Hot side—250 °C Cold side—175 °C
Width	62 mm
Length	62 mm
Height	4 mm

2.3. Variable Conductance Vapour Chambers

The VCs in the system are part of the ongoing project CoolSpot (see acknowledgements). These VCs act as thermal controllers as they transport the heat excess to areas where the limit temperature is not reached. Since the purpose is to prevent the TEGs from overheating, the boiling temperature of the working fluid must be as close as possible to the maximum temperature of the TEGs' hot face. To achieve the main thermal control purpose, keep the TEGs hot face closest to its maximum tolerated temperature, and to address the volatile thermal loads present in the exhaust gases, these VCs are pressurised with a non-condensable gas, with an adjusted pre-load pressure for a boiling temperature of the working fluid slightly above the TEGs' maximum temperature so that the hot face temperature will be close to this maximum, maximising output. With water as a working fluid, this pressure would be around 4 MPa, however, the materials used here would recommend a fluid with saturation pressures at the designed temperature which would be closer to ambient. Such fluid could be the Dowtherm-A, which has a saturation pressure around ambient for 250 °C.

Enhanced Surfaces

Laser textured VCs can be a considerable advantage when compared to common HPs and VCs. The idea is to implement this technique for a better boiling and condensation performance and also to replace the wick, responsible for returning the fluid from the condenser to the evaporator, by a textured surface. This approach has already been introduced in [19].

On the one hand, an important approach to boiling enhancement is the creation of micro/nanochannels and cavities by laser ablation, triggering the onset of nucleate boiling with lower wall superheat, therefore, bubbles can be formed with lower superheat, avoiding a high bubble growth rate. The ideal size of the nucleation cavities are a function of local wall and bulk fluid temperatures, heat transfer coefficient and heat flux [20]. Another aspect is the wettability of the surface. For this purpose, hydrophobic surfaces promote larger bubble departure diameters and more coalescence, which reduces the temperature of the onset of nucleate boiling and increases the heat transfer coefficient. On the contrary, hydrophilic surfaces provide smaller bubble departure diameters as the surface "pulls" the liquid towards the nucleation sites, which requires greater superheat for nucleate boiling to occur and do not necessarily provide an enhanced heat transfer coefficient at low heat fluxes [21]. Despite the fact that hydrophobic surfaces seem to be better at first sight, the capillarity of the texture should also be considered, as it is responsible for the movement of the condensed liquid back to the evaporator [22].

On the other hand, steam condensation can happen in two distinct ways: dropwise condensation and film condensation. In dropwise condensation, vapour droplets form at an acute angle to a surface, flowing as they tend to coalescence and accumulate static droplets. For film condensation, a thin laminar film of liquid is created covering the surface and tends to increase as the liquid flows and accumulates. The heat transfer coefficient for dropwise condensation can be one order of magnitude higher than that of film condensation ([23]), making it more desirable. Although for long periods of time it is common that a film would start to occur ([24]), dropwise condensation is more effective because drops are formed and released, keeping the surface continually exposed instead of creating a thermal resistance barrier that would cover the surface–film condensation. For a practical appliance, one of the necessary conditions for dropwise condensation would be the creation of a hydrophobic contact, so that liquid droplets would tend to compact, instead of spreading and accumulating in a film [25–27]. One of the methods to create metallic hydrophobic surfaces is by laser ablation, with or without chemical treatment.

Another important aspect of this improvement is capillarity, which is behind the movement of the working fluid from the condenser to the evaporator. Capillarity action is caused by the minimisation of the surface energy, in other words, the smaller the contact angle of the fluid with the surface the higher the capillarity. Consequently, hydrophilic surfaces or paths are desirable, so the fluid can spread and move along its way [28].

Concluding, in order to achieve better condensation and evaporation, the surface must have the biggest contact angle possible with the fluid (hydrophobic), but, in an opposite way, the movement of the fluid as it condenses and returns to the evaporator must have the smallest contact angle possible. As is evident, there is a conflict in the idealisation of the wettability of the surface. In order to overcome this problem, a biphilic surface is being idealised, where the main pattern is hydrophobic and there are hydrophilic paths. This can be achieved with multimaterial surfaces, that are being tested by the authors via laser ablation and laser sintering, through Nd-YAG 04 and LM-DVO 100 laser machines, respectively, with some sample results having been presented in [19]. These considerations do not affect the present modelling, as the phase change phenomena is treated in a simplified way, with the vapour region of the VCs being considered isothermal and the NCG region being treated as adiabatic.

2.4. Cooling Plates

The CP design used is based on the CPs manufactured by the authors from commercially available heat sinks obtained by the extrusion process, to which a cover has been welded. These CPs have a high fin density, which minimises their thermal resistance, and a large flow cross-section to minimise pressure drop. This is not the focus of the present analysis and other lighter, more compact designs could have been chosen for the simulation. Indeed, it is expected that an industrial prototype will be much lighter and compact. However, this geometry was used to allow future experimental validation of the simulations. The CPs have a typical working operation, water flows through the channels ensuring the cold face of the TEGs stays as cool as possible. The CP channels implemented a Fischer Elektronik SK624 ([29]) profile inside an aluminium case, which, due to its thickness, allows the uniform temperature of the TEGs cold face.

3. Heavy Duty Vehicle

The realistic simulation of the performance of a TCTG applied to an HDV during a driving cycle requires the prediction of the HDV operation during that cycle. Namely, it is necessary to predict the engine load and speed required to perform the driving cycle and the resulting exhaust temperature and flow rate along the duration of the driving cycle. Thus, an HDV vehicle was simulated through AVL Cruise and Boost software tools. The engine and vehicle main parameters are presented in Table 2. All data regarding the HDV engine were obtained from the literature ([30]), which represents a common engine for these vehicles. This data is interpolated by the software with the given cycle run constrains. In order to acquire the combination simulation of power performance, fuel economy and exhaust gas temperature and mass flow rate the vehicle model present in Figure 3 was used. This is an AVL template of a class five commercial truck where the components had to be defined. A component "AVL exhaust system" was implemented into the model to allow exhaust flow computations. This component connects an exhaust aftertreatment system created in AVL Boost with the Cruise simulation.

Table 2. Main design features of the test vehicle—adapted from [30].

Heavy Duty Vehicle	
Tractor Curb/Gross Weigh	7050/7500 kg
Frotal Area	10.28 m^2
Trailer Curb/GrossWeight	7500/25,500 kg
Cycle	4 strokes
Displacment	15.99 L
Number of cylinders	6
Valves per cylinder	4
Fuel	Diesel
Fuel Heating Value	44,000 kJ/kg
Fuel injection system	Common-rail
Engine speed range	[800–2000] rpm
Maximum power	384 kW (515 hp)
Maximum torque	2292 N·m 1200 at rpm

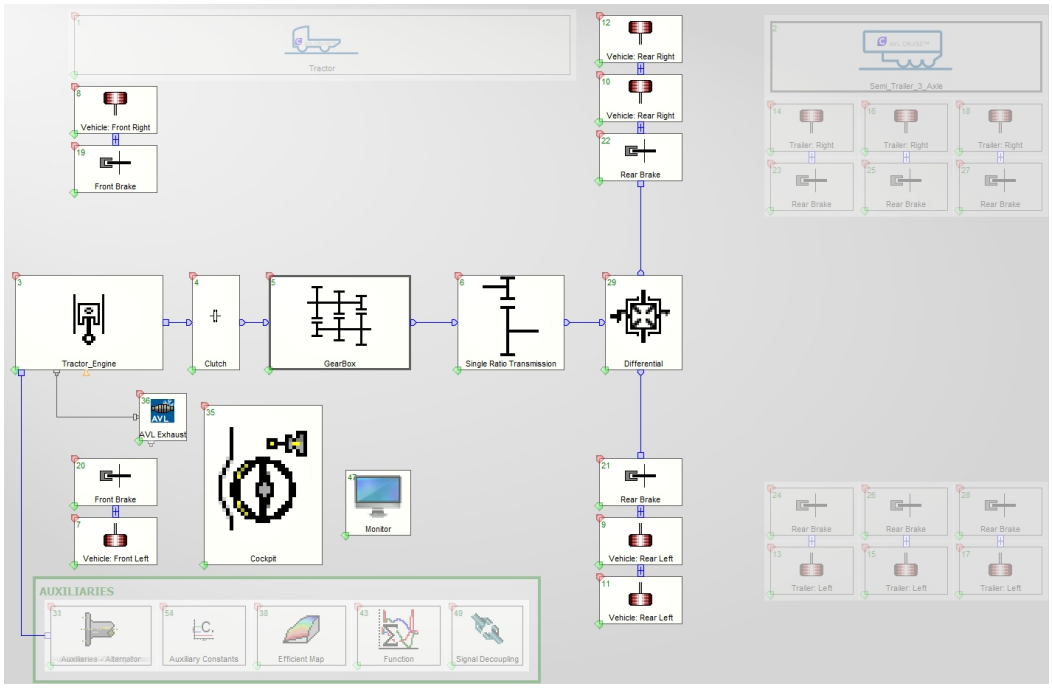

Figure 3. HDV CRUISE setup.

Cycle Runs

Two cycle runs were tested, WHVC, Figure 4, and a Long Haul cycle, Figure 5. The WHVC, usually used for HDV certification, was obtained from the literature and introduced in CRUISE. In the Long Haul cycle run, available in the CRUISE libraries, the HDV reaches a maximum velocity of 85 km/h along 100 km with different inclinations. This cycle was also simulated because, besides the fact that HDVs travel very long distances, it can represent a regional delivery with a longer distance than WHVC, aiding the visualisation of the heat exchanger performance. The simulations with the WHVC were performed with three trailer weight loads, 25.5 t (full), 12.75 t (half) and 7.5 t (empty). As for the Long Haul, the gross weight of the trailer was applied.

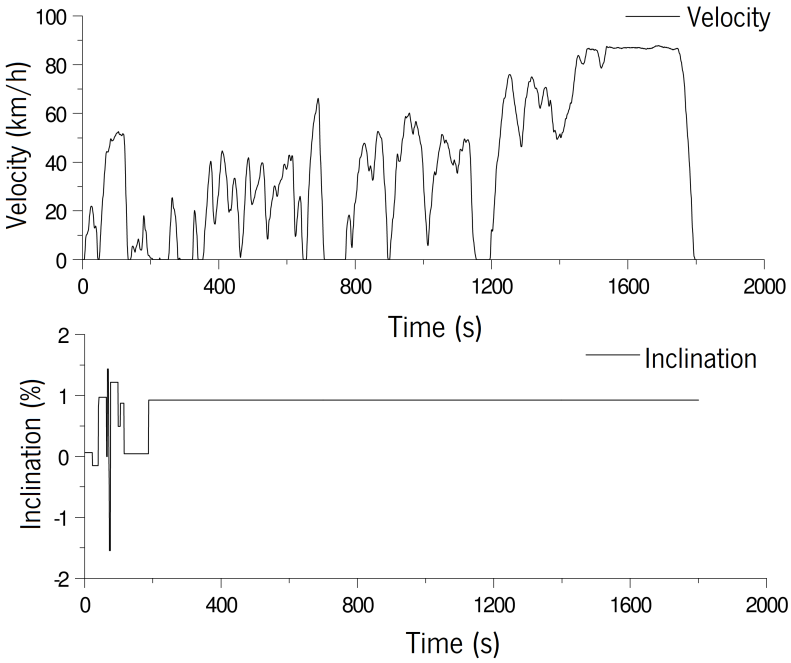

Figure 4. WHVC parameters.

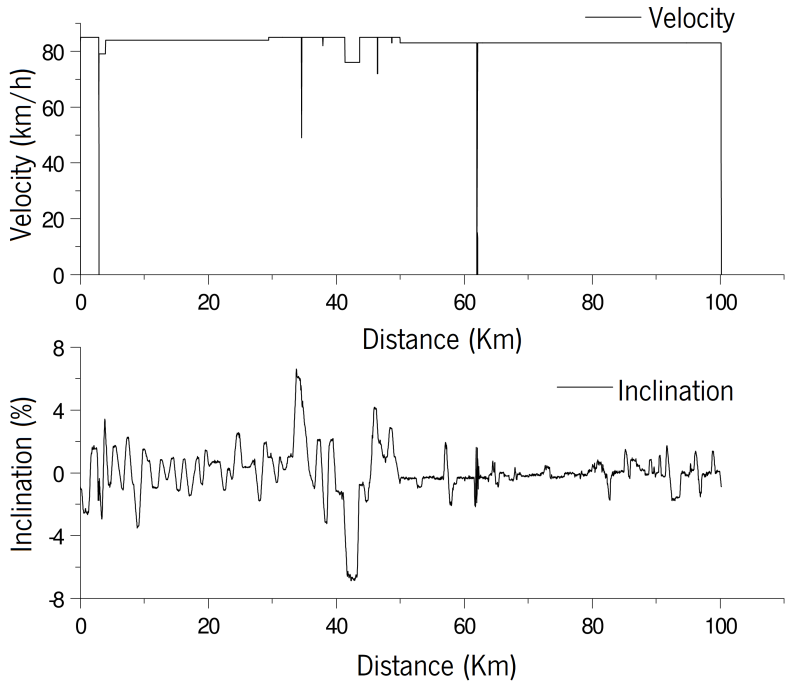

Figure 5. Long Haul cycle run parameters from AVL software.

4. System Simulations

4.1. Heat Flux

The TEG model implements discretizations along the flow direction and across the heat exchanger layers. Both these discretizations are one-dimensional in nature and connected through energy balances. However, the three-dimensional effects were taken into account by obtaining the 1D equivalent thermal resistances of the 3D shapes and then incorporating these thermal resistances into the heat transfer analysis. These simulations were performed for fixed heat sources and heat sink conditions, but the thermal resistances extracted from the analysis are universal, as they mainly depend on geometric parameters.

This analysis was executed through a two-dimensional steady-state thermal analysis in COMSOL Multiphysics. The CAD model of the system, the respective component materials and their thermal properties, and convective properties, such as the heat transfer coefficient of the WFs, were applied to the simulation. Two distinct heat transfer modes are possible for each heat exchanger section: VCs are treated as isothermal cavities, when phase change is present, and VCs are treated as adiabatic cavities when only NCG is present and no vapour. Thus, two different simulations were performed. In these simulations, data from cycle points regarding the exhaust gas were implemented. For the isothermal VCs (active, phase change region), a cycle point where the module body would exceed the limit temperature of 250 °C without the aid of phase change. For the adiabatic VCs (inactive, NCG region), a cycle point in which the modules would not exceed the limit temperature was selected.

4.2. 1D Model

To predict the behaviour of the concept, an algorithm accounts for the thermal and electrical properties of the several components, taking into consideration the status of the VCs in each discretized section and providing the fundamental results for the optimisation of the system. For the heat exchanger analysis, both the TEGs hot face (T_{TEG_h}) and cold face (T_{TEG_c}) must be calculated for each cycle point. Since the main objective of the present study was to assess the performance of the thermal control strategy rather than to assess and optimise specific TEG materials or geometries, the approach taken to model the thermoelectric modules was simplified. Regarding the electrical load resistances, matched load conditions were considered. The prediction of the behaviour of the TEGs, namely the power output and their effective thermal resistance was fitted from datasheet information for matched load conditions. This way, the heat flux already accounts for the average effect of the Peltier heat pumping. The power prediction was computed from polynomial regression of the power curves interpolated for the actual hot side and cold side temperatures obtained from the heat transfer calculations.

Regarding the power electronics to be implemented in a real prototype a maximum power point tracking (MPPT) system should be implemented along with a voltage buck/boost strategy to allow the supply of the electricity with a voltage level compatible with the system. It is expected that the thermal control will be beneficial for temperature matching among TEG rows. Given the sequential activation of the several rows of the system according to the thermal input, a modular architecture is probably better suited than a centralised one.

The heat exchanger is divided into several longitudinal slices in which the heat transfer calculations are performed in 1D. Energy balances are performed to each section and a calculation of vaporisation or condensation power is also performed if the VCs happens to be active. In the first iteration of a slice, it is considered that there is no excess heat and that the VCs are not operating (no phase change). Under these conditions, the thermal resistances with adiabatic VCs are applied. Then, on that slice, there is the need to discover if there is there is heat excess or not. If the heat transfer calculations confirm that indeed there is no excess temperature (T_{TEG_h} < 250 °C), the VCs are indeed not operating and the thermal resistances with adiabatic VCs have been correctly applied. Otherwise, if the calculations confirm that there is an excess temperature (T_{TEG_h} > 250 °C), the VCs are in reality operating and absorbing heat so that T_{TEG_h} does not exceed the operating temperature limit. Therefore, the calculation must be repeated, now using the thermal resistances considering isothermal VCs. Under these conditions, a computation of the heat accumulated by the VCs in the form of vapour is performed. Additionally, there is a third possibility, in which the calculations confirm that the temperature would be below the temperature limit without the VCs being active, but the accumulated excess power that has been calculated from the sections located upstream (which represents vapour generated and accumulated) has still not been absorbed by the subsequent slices. This would mean that the slice is located in a condensation region of the VCs. Here, the calculations are redone, but now using the isothermal VCs condition and calculating the heat that has been

absorbed by the VCs. Once all accumulated excess heat has been absorbed by subsequent sections and depleted, then all downstream sections will operate without phase change, and a T_{TEG_h} lower than the limit of the materials.

The algorithm not only provides a prediction of the electrical load produced by the modules and how many TEG lines are fully active during the cycle run, but also the power absorbed by the heat exchanger and by the TEGs and the pumping power necessary to overcome the TCTG by the exhaust gas.

5. Results and Discussion

On account of the simulation environments and algorithm previously described, it was possible to fully analyse the main outputs under the selected operating conditions and provide a suitable set up for the TCTG system. The proposed model has a total of 128 commercial TEGs, GM250-127-28-10 ([18]), which withstand a maximum temperature of 250 °C. This system follows the stacked setup presented in Figure 6. It should be noted that the volumetry of this concept is not optimised. Namely, an industrial design will display a much lower volume and mass. For this reason, the actual mass of the design was still not considered into the analysis as it will be much lower.

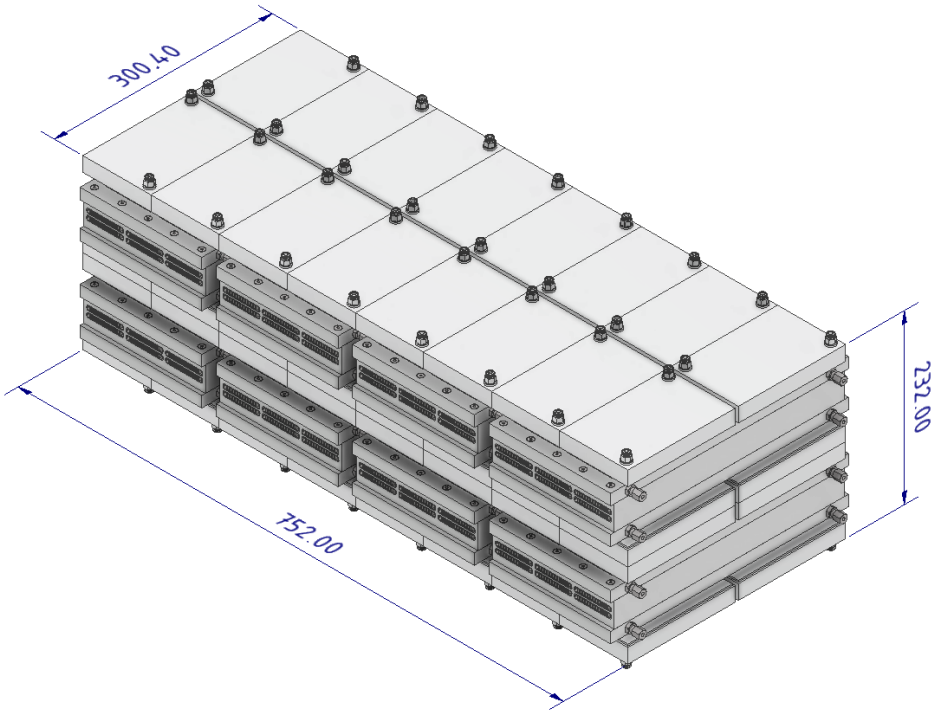

Figure 6. Proposed system CAD model (dimensions in mm).

5.1. Heavy Duty Vehicle Simulation Results

Figures 7 and 8 provide the HDV simulation results regarding the exhaust gas temperature and mass flow rate, respectively, for the full weight WHVC. The heterogeneous behaviour of the exhaust load is noticeable. The highly dynamic exhaust profile makes the temperature control characteristic of the TEG system crucial. Moreover, it is obvious that the temperature of the exhaust gas is usually higher than the maximum operating temperature of the modules, 250 °C. When in a WHVC cycle run with a full load, the HDV reached the 464 °C .

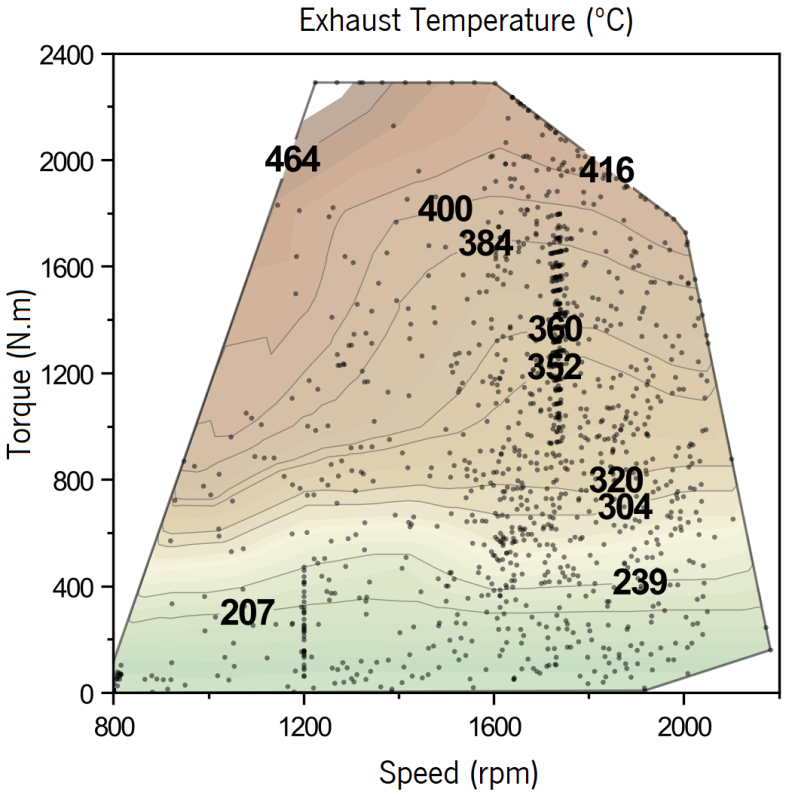

Figure 7. Exhaust gas contour map: exhaust gas temperature at the aftertreatment outlet.

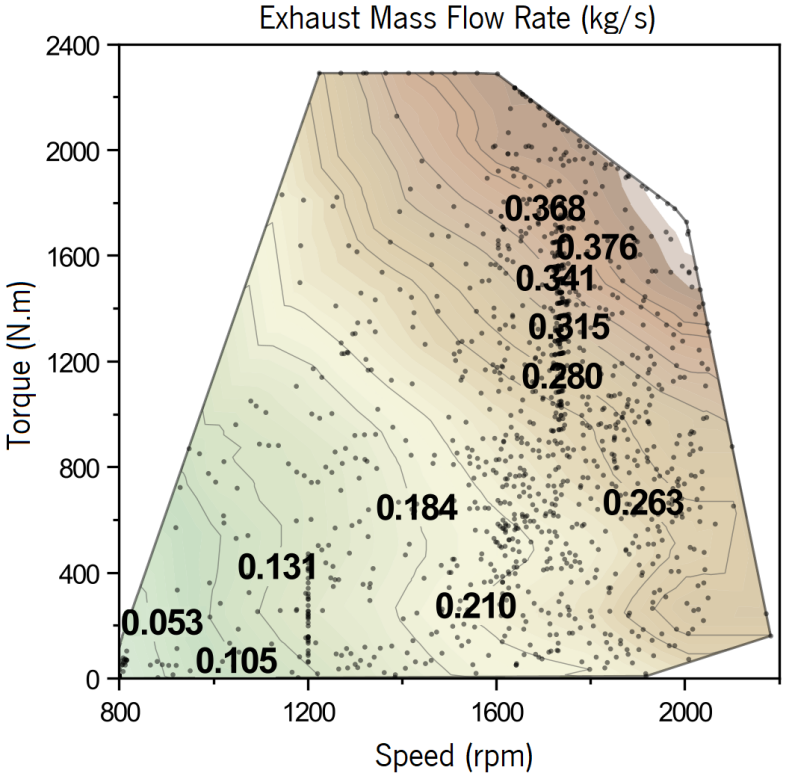

Figure 8. Exhaust gas contour map: exhaust gas mas flow rate at the aftertreatment outlet.

5.2. Temperature and Heat Distribution

The thermal control is ensured by the VCs as they spread the excess heat from the hotter regions of the heat exchanger to the colder regions, where the deficit thermal load does not allow the TEGs to operate near their maximum allowed temperature. To illustrate this process, two cycle points under the fully loaded WHVC cycle with low and high exhaust thermal load are illustrated in Figures 9 and 10, where the temperature profiles and thermal power variation along the heat exchanger length for WHVC cycle run under two cycle points: 187s (low thermal load) and 1296s (high thermal load) are presented. It is possible to see the thermal behaviour from the inlet to the outlet of the heat exchanger. Figure 9 demonstrates the system temperatures, while Figure 10 represents the heat fluxes behaviour.

In the low thermal load graphics, it is clear that the VCs act as adiabatic bodies since the exhaust gas and TEGs hot face temperatures are very close and do not come near the maximum TEGs working temperature, thus the heat flux is fully absorbed by the heat exchanger. In this cycle point, the TEGs do not work at their optimal temperature, as no sufficient heat was absorbed or accumulated by the system in order to compensate for this lack of thermal power. As expected, due to the low thermal load, the cooling water hardly changes its temperature. In the high thermal load cycle point, the VCs are active along the first 17 cm of the heat exchanger. Initially, the VCs are absorbing the excess heat (0–5 cm), which is then released in the following active VCs section (between 5 and 17 cm), visualised in Figure 10. By absorbing the heat, the VCs are preventing the TEGs hot face from overheating, while releasing the absorbed heat in the colder area located downstream, which without the VCs would be under-heated. Therefore, not only is there no overheating, but there are more TEGs working at their non-optimal temperature because of the heat spreading feature. This thermal control results in the temperature profile presented in Figure 9. By absorbing the excess thermal load, the exhaust gas temperature is reduced to the TEGs optimal temperature, which is kept due to the release of the excess heat flux along the deficit area. However, a temperature drop is observed in the TEGs hot face (from 17 cm until the end of the heat exchanger) because the deficit region consumed all the heat released from the VCs, which are no longer spreading any thermal load, and therefore, are inactive.

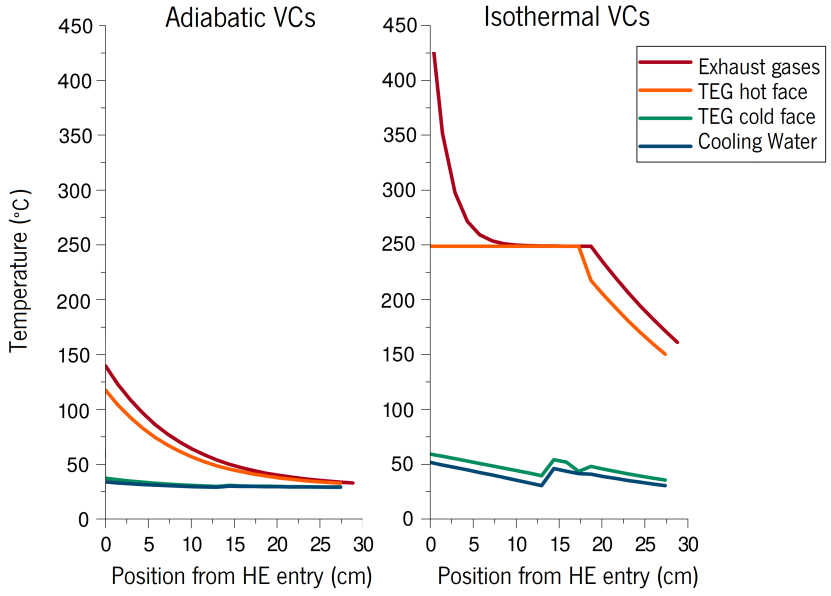

Figure 9. Sample temperature balance performed to the vapour chambers along the length of the Heat Exchanger, for a low thermal load (Adiabatic VCs) (WHVC FULL 187s) and a high thermal load event (Isothermal VCs) (WHVC FULL 1296s), with detail of the heat absorbed (corresponding to vaporisation), heat released (corresponding to condensation) and heat accumulation (net vapour mass accumulated).

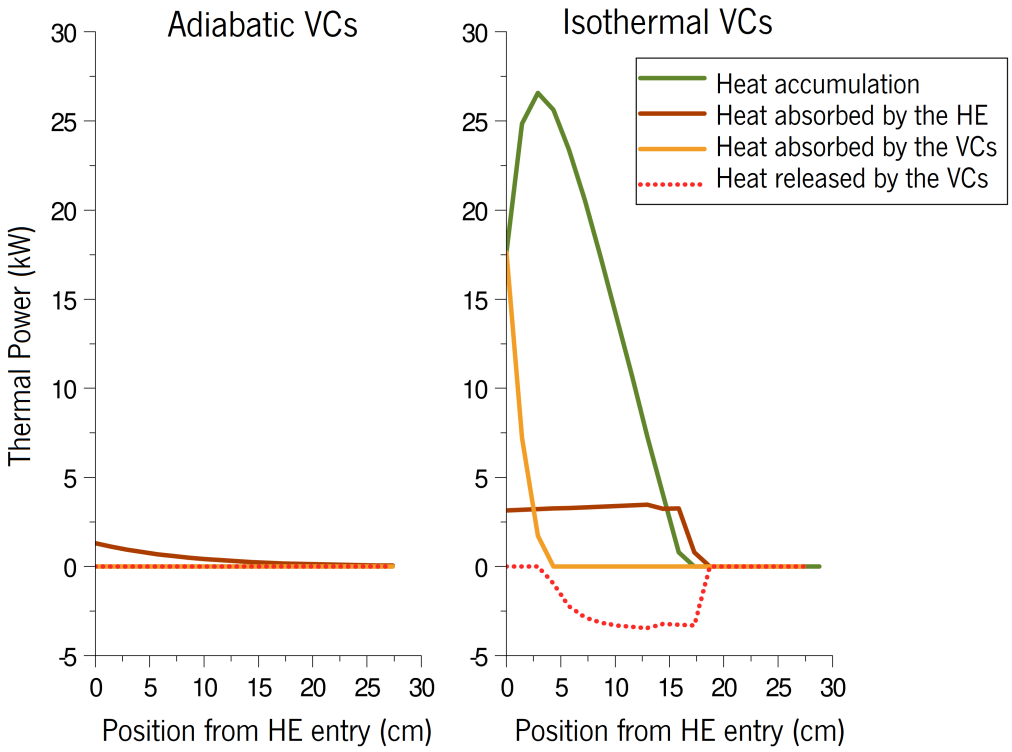

Figure 10. Sample thermal power balance performed to the vapour chambers along the length of the heat exchanger, for a low thermal load (Adiabatic VCs) (WHVC FULL 187s) and a high thermal load event (Isothermal VCs) (WHVC FULL 1296s), with detail of the heat absorbed (corresponding to vaporisation), heat released (corresponding to condensation) and heat accumulation (net vapour mass accumulated).

5.3. Power Distribution along TEG Rows

When the thermal level absorbed by the heat exchanger is lower than the maximum operating temperature of the TEGs, all the heat will reach the TEGs by conduction across the heat exchanger, since the VCs are not active. Otherwise, the VCs start absorbing the excess heat by vaporisation, preventing the rise of the temperature above the established limit. The accumulated vapour inside the VCs condensates in the cooler regions, heating them. This thermal control results in different thermal loads achieving the TEGs without ever overheating them, thus varying the thermal output along the TEG rows. The graphic in Figure 11 graphics shows the thermal power distribution along the several TEG rows along the exhaust flow direction. The stabilisation of the electrical outputs, mostly on the first and second TEG rows, reflects the moment when the maximum operating temperature is reached at the hot face of all modules of that row. This means that the VCs are filled with vapour in that location and are absorbing (vaporisation) excess thermal power or releasing (condensation) power that had been accumulated upstream, as the TEGs hot face is kept constant. The second TEGs row achieved higher electrical outputs since the cooling plates are in counter-current flow, and thus, the second row has lower coolant temperature than the first one (each cooling plate encompasses modules in two rows). In the subsequent rows, the VCs have depleted all the excess heat accumulated in previous rows, therefore, the TEGs are no longer working near their maximum operating temperature. Essentially, the next row will start increasing its power generation rate, once the previous one has achieved its maximum operation.

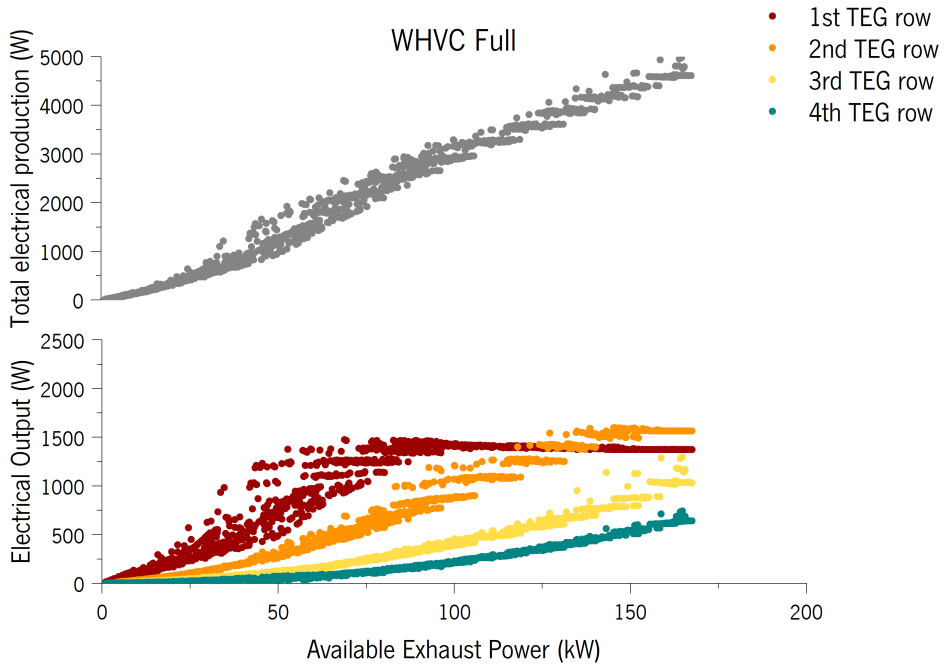

Figure 11. Power distribution along the system modules for WHVC driving cycle with 25.5 t.

5.4. Electrical Production

A possible evaluation of the system performance is the analysis of the electrical generation and the thermal power absorbed by the heat exchanger, during the driving cycles. It was predicted that the system has not only an efficient thermal control of the heat exchanger but also the ability of electricity generation under different thermal loads. Figure 12 displays the available exhaust thermal power, the exhaust power absorbed by the heat exchanger and the electrical output along the WHVC with full weight load.

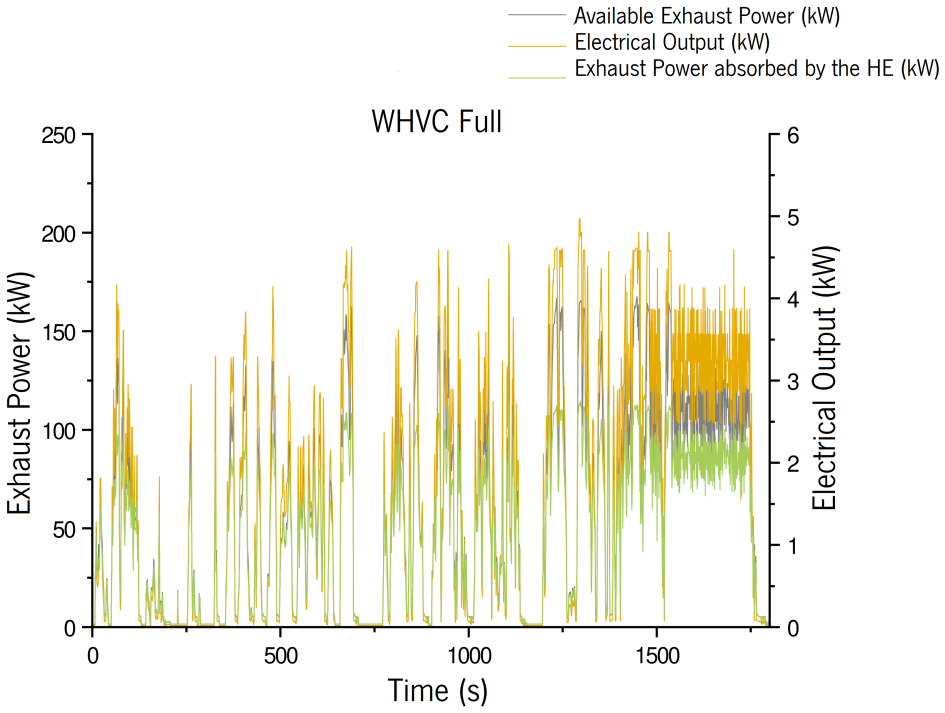

Figure 12. Results of the TEGs generated power, absorbed exhaust power and the available exhaust power for WHVC driving cycle with 25.5 t.

5.5. System Savings

The vehicle alternator/motor generator and the battery support all the electrical loads of the HDVs. The increasing electrical demand present in the modern commercial transportation, such as the electronic engine and emissions control systems, gauges, air conditioning, air-compressor, and lights are accountable for decreasing the fuel efficiency. Most commercial HDV alternators have near 2.5 kW of electrical loads when operating, which for an alternator such as the 36SI HD Alternator ([31]) with an efficiency of 68% results in a total of 3.7 kW of mechanical power consumption, representing more than 12 kW of fuel power in an engine with an average mechanical efficiency of 30%. In Table 3, the fundamental savings obtained by applying the TEG system are presented assuming the mentioned alternator with 68% efficiency for both cycle runs, Long Haul and WHVC with different loads. It was considered that the alternator was being fully used along the entire cycle runs. Along the Long Haul cycle, the system can almost produce enough average electric power to fully compensate the alternator power needs by producing nearly 2.5 kW, resulting in a fuel saving of 1.07 L/100 km and reducing the CO_2 emissions by 28.75 g/km. In respect to the WHVC cycle run, the electrical production does not completely meet the alternator requirements, especially in the cycle with the lightest weight, with an average of 1.2 KW in contrast to the necessary 2.5 kW. However, this cycle run has fuel saving rates close to the Long Haul ones. This is justified due the lower WHVC engine efficiencies on which the savings in the mechanical power requirements cause proportionally higher fuel savings.

Table 3. Average maximum engine power savings from applying the developed TEG system within the several cycle runs.

	Average Values				**Maximum Engine Power**			
	Long Haul	**WHVC 7.5 t**	**WHVC 12.75 t**	**WHVC 25.5 t**	**Long Haul**	**WHVC 7.5 t**	**WHVC 12.75 t**	**WHVC 25.5 t**
Driving Cycle Data								
Distance [km]	100	20	20	20	-	-	-	-
Engine efficiency [%]	34	28	29	30	38	39	39	41
Required Mechanical Power [kW]	173	102	108	141	382	378	378	384
Applying the TEG System								
Electric energy produced [kw]	2.4	1.24	1.3	1.63	3.83	3.93	4.24	4.77
Energy produced [kJ/km]	101	112	117	147	-	-	-	-
Required Mechanical Power [kW]	169	100	106	138	375	378	378	384
Fuel savings [L/100 km]	1.14	1.33	1.37	1.64	0.004	0.002	0.002	0.002
Fuel savings [%]	2.06	2.14	2.1	2.02	1.76	1.78	1.78	1.84
CO2 emissions savings [g/km]	30.45	35.57	36.68	43.92	0.01	0.06	0.06	0.06

6. Conclusions

The goal of the present study was to evaluate a typical long haul commercial heavy-duty vehicle (HDV) equipped with the thermoelectric exhaust heat recovery system with thermal control proposed by the authors. The purpose of the system is to maximise the absorption of the heat normally lost through the exhaust gases and convert it into electricity using thermoelectric generators operating at an optimised temperature level irrespective of engine load. A previously proposed custom thermoelectric and heat transfer modelling was run based on AVL Cruise driving cycle analysis results under the WHVC and long haul driving cycles, and adapted to a new geometry consisting of wavy fin heat exchanger and Variable Conductance Vapour Chambers (VCs). This latter component was used to implement the absorption and spreading of excess heat from overheated regions to under-heated regions of the heat exchanger with an optimised temperature through liquid/vapour phase change.

The accomplished project results of the developed TEG system regarding the electricity production, fuel savings and corresponding CO_2 emission savings seem overall promising, especially when compared with existing results in literature for thermoelectric generators. Average electric power productions of 1.63 kW, 1.3 kW, 1.24 kW were achieved for the WHVC Full, Half and Empty, respectively, and 2.4 kW for the Long Haul cycle run. The maximum electrical powers were similar in the four cases since the same modules were used: 4.98 kW,

4.77 kW, 4.62 kW for WHVC Full, Half and Empty, respectively, and 4.63 kW for the Long Haul cycle run, meaning that at these points of the cycle the TEGs were operating at their optimal working temperature, 250 °C. Average fuel consumption savings of about 2% and CO_2 emissions savings of around 37 g/km were predicted in most simulations. It is possible to conclude that the system has a good potential for waste recovery applications in HDVs with minimum maintenance requirements, especially when submitted to long vehicle use. This very positive performance of the system is attributed to the ability of the system to maximise heat absorption, while still keeping the modules close to their optimal temperature while preventing them from overheating or from excessive thermal dilution.

Author Contributions: Conceptualization, C.C.S. and F.P.B.; methodology, C.C.S. and F.P.B.; software, C.C.S. and F.P.B.; validation, C.C.S. and F.P.B.; formal analysis, C.C.S. and F.P.B.; investigation, C.C.S. and F.P.B.; resources, Ó.C. and F.P.B.; data curation, F.P.B.; writing—original draft preparation, C.C.S., M.C. and F.P.B.; writing—review and editing, C.C.S., Ó.C., M.C., A.S.M. and F.P.B.; visualization, C.C.S., M.C. and F.P.B.; supervision, F.P.B. and J.M.; project administration, F.P.B., Ó.C. and A.S.M.; funding acquisition, F.P.B. All authors have read and agreed to the published version of the manuscript.

Funding: This article was partially supported by projects COOLSPOT PTDC/EME-TED/7801/2020, UIDB/00481/2020 and UIDP/00481/2020 (Centre for Mechanical Technology and Automation—TEMA) and UIDB/04077/2020 (MEchanical Engineering and Resource Sustainability Center—MEtRICs)—Fundação para a Ciência e a Tecnologia (FCT); CENTRO-01-0145-FEDER-022083 (Centro2020), Norte2020, Compete2020, under the PORTUGAL 2020 Partnership Agreement, through Portuguese national funds of FCT/MCTES (PIDDAC) and the European Regional Development Fund.

Institutional Review Board Statement: Not applicable.

Informed Consent Statement: Not applicable.

Data Availability Statement: Not applicable.

Acknowledgments: The authors wish to acknowledge the funding agencies and programmes mentioned in Funding (see above). The authors also wish to acknowledge the support of BORGWARNER Emissions systems (Vigo Technical Center) for providing the wavy fins that were the assessed in the present analysis, and also AVL List GmbH for the AVL SUITE license provided to MEtRICs/UM under the University Partnership Program.

Conflicts of Interest: The authors declare no conflict of interest. The funders had no role in the design of the study; in the collection, analyses, or interpretation of data; in the writing of the manuscript, or in the decision to publish the results.

Abbreviations

The following abbreviations/acronyms are used in this manuscript:

AVL BOOST	Engine simulation software part of AVL Suite from Company AVL List GmbH
AVL CRUISE	Driving cycle simulation software part of AVL Suite from Company AVL List GmbH
CP	Cooling Plate
HDV	Heavy-duty Vehicle
HPs	Heat pipes
MPPT	Maximum power point tracking
NCG	Non-condensable gas
TCTG	Temperature-controlled thermoelectric generator
TEG	Thermoelectric generators
TS	Thermosiphons
VC	Vapour chambers
VCHP	Variable conductance heat pipes
VCTS	Variable conductance thermosiphons
VCVC	Variable conductance vapour chamber
WF	Wavy fins
WHVC	World Harmonized Vehicle Cycle

References

1. Georgatzi, V.V.; Stamboulis, Y.; Vetsikas, A. Examining the determinants of CO_2 emissions caused by the transport sector: Empirical evidence from 12 European countries. *Econ. Anal. Policy* **2020**, *65*, 11–20. [CrossRef]
2. Holmberg, K.; Andersson, P.; Nylund, N.O.; Mäkelä, K.; Erdemir, A. Global energy consumption due to friction in trucks and buses. *Tribol. Int.* **2014**, *78*, 94–114. [CrossRef]
3. Heber, L.; Schwab, J.; Knobelspies, T. 3 kW Thermoelectric Generator for Natural Gas-Powered Heavy-Duty Vehicles—Holistic Development, Optimization and Validation. *Energies* **2022**, *15*, 15. doi: 10.3390/en15010015 [CrossRef]
4. Rodriguez, R.; Preindl, M.; Cotton, J.S.; Emadi, A. Review and Trends of Thermoelectric Generator Heat Recovery in Automotive Applications. *IEEE Trans. Veh. Technol.* **2019**, *99*, 5366–5378. [CrossRef]
5. Heber, L.; Schwab, J. Modelling of a Thermoelectric Generator for Heavy-Duty Natural Gas Vehicles: Techno-Economic Approach and Experimental Investigation. *Appl. Therm. Eng.* **2020**, *174*, 115–156. [CrossRef]
6. Brito, F.P.; Vieira, R.; Martins, J.; Goncalves, L.M.; Goncalves, A.P.; Coelho, R.; Lopes, E.B.; Symeou, E.; Kyratsi, T. Analysis of thermoelectric generator incorporating n-magnesium silicide and p-tetrahedrite materials. *Energy Convers. Manag.* **2021**, *236*, 114003. [CrossRef]
7. Brito, F.P.; Peixoto, J.S.;Martins, J.; Gonçalves, A.P.; Louca, L.; Vlachos, N.; Kyratsi, T. Analysis and Design of a Silicide-Tetrahedrite Thermoelectric Generator Concept Suitable for Large-Scale Industrial Waste Heat Recovery. *Energies* **2021**, *14*, 5655. [CrossRef]
8. Brito, F.P.; Martins, J.; Goncalves, L.M.; Sousa, R. Temperature controlled exhaust heat thermoelectric generation. *SAE Int. J. Passeng. Cars Electron. Electr. Syst.* **2012**, *5*, 561–571. doi: [CrossRef]
9. Brito, F.P.; Martins, J.; Hançer, E.; Antunes, N.; Gonçalves, L.M. Gonçalves Thermoelectric Exhaust Heat Recovery with Heat Pipe-Based Thermal Control. *J. Electron. Mater.* **2015**, *44*, 1984–1997. [CrossRef]
10. Brito, F.P.; Alves, A.; Pires, J.M.; Martins, L.B.; Martins, J.; Oliveira, J.; Teixeira, J.; Goncalves, L.M.; Hall, M.J. Analysis of a Temperature-Controlled Exhaust Thermoelectric Generator During a Driving Cycle. *IEEE J. Electron. Mater.* **2016**, *45*, 1846–1870. [CrossRef]
11. Brito, F.P.; Martins, J.; Goncalves, L.M.; Antunes, N.; Sousa, D. Influence of heat pipe operating temperature on exhaust heat thermoelectric generation. *SAE Int. J. Passenger Cars Mech. Syst.* **2013**, *6*, 652–664. doi: [CrossRef]
12. Brito, F.P.; Pacheco, N.; Vieira, R.; Martins, J.; Martins, L.; Teixeira, J.; Goncalves, L.M.; Oliveira, J.; Hall, M.J. Efficiency improvement of vehicles using temperature controlled exhaust thermoelectric generators. *Energy Convers. Manag.* **2020**, *203*, 112255. [CrossRef]
13. Pacheco, N.; Brito, F.P.; Vieira, R.; Martins, J.; Barbosa, H.; Goncalves, L.M. Compact automotive thermoelectric generator with embedded heat pipes for thermal control. *Energy* **2020**, *197*, 117–154. [CrossRef]
14. Kale, S.S.; Bhatkar, V.W.; Dange, M.M. Performance Evaluation of Plate-Fin-And Tube Heat Exchanger with Wavy Fins—A Review. *J. Eng. Res. Appl.* **2014**, *4*, 154–158.
15. Tsai, M.C.; Kang, S.W.; de Paiva, K.V. Experimental studies of thermal resistance in a vapor chamber heat spreader. *Appl. Therm. Eng.* **2013**, *56*, 38–44. [CrossRef]
16. Junqi, D.; Jiangping, C.; Zhijiu, C.; Yimin, Z.; Wenfeng, Z. Heat transfer and pressure drop correlations for the wavy fin and flat tube heat exchangers. *Appl. Therm. Eng.* **2007**, *27*, 2066–2073. [CrossRef]
17. Fin Manufacturer, Advanced Fin UK, Wavy Fin. Available online: http://advancedfinuk.com/wavy.htm (accessed on 21 December 2021).
18. Adaptive. *GM250-127-28-10 Thermoelectric Generator Module*; European Thermodynamics Limited: Leicestershire, UK, 2017.
19. Moita, A.S.; Pontes, P.; Martins, L.; Coelho, M.; Carvalho, O.; Brito, F.P.; Moreira, A.L.N. Complex Fluid Flow in Microchannels and Heat Pipes with Enhanced Surfaces for Advanced Heat Conversion and Recovery Systems. *Energies* **2022**, *15*, 1478. [CrossRef]
20. Kandlikar, S.G. High Flux Heat Removal with Microchannels—A Roadmap of Challenges and Opportunities. *Heat Transf. Eng.* **2005**, *26*, 5–14. [CrossRef]
21. Teodori, E.; Valente, T.; Malavasi, I.; Moita, A.S.; Marengo, M.; Moreira, A.L.N. Effect of extreme wetting scenarios on pool boiling conditions. *Appl. Therm. Eng.* **2017**, *115*, 1424–1437. [CrossRef]
22. Zupančič, M.; Može, M.; Gregorčič, P.; Golobič, I Nanosecond laser texturing of uniformly and non-uniformly wettable micro structured metal surfaces for enhanced boiling heat transfer. *Appl. Surf. Sci.* **2017**, *399*, 480–490. [CrossRef]
23. Lou, D.; Mei, S.; Wang, B.; Li, T.; Cao, J.; Yang, Q.; Tao, Q.; Cheng, J.; Liu, D. Effect of stabilizing heat treatment on condensation heat transfer performance of laser micro-/nano-textured copper surface. *J. Mater. Sci.* **2021**, *56*, 3981–3994. [CrossRef]
24. Pandey, S. Dropwise and filmwise condensation. *Int. J. Sci. Eng. Res.* **2012**, *3*, 1–5.
25. Ahlers, M.; Buck-Emden, A.; Bart, H.J. Is dropwise condensation feasible? A review on surface modifications for continuous dropwise condensation and a profitability analysis. *J. Adv. Res.* **2019**, *16*, 1–13. [CrossRef] [PubMed]
26. Darband, G.B.; Aliofkhazraei, M.; Khorsand, S.; Sokhanvar, S.; Kaboli, A. Science and engineering of superhydrophobic surfaces: review of corrosion resistance, chemical and mechanical stability. *Arab. J. Chem.* **2020**, *13*, 1763–1802. [CrossRef]
27. Ellinas, K.; Tserepi, A.; Gogolides, E. Durable superhydrophobic and superamphiphobic polymeric surfaces and their applications: A review. *Adv. Colloid Interfac.* **2017**, *250*, 132–157. [CrossRef] [PubMed]
28. Jokinen, V.; Franssila, S. Capillarity in microfluidic channels with hydrophilic and hydrophobic walls. *Microfluid. Nanofluid.* **2008**, *5*, 443–448. [CrossRef]

29. Fischerelektronik. Standard Extruded Heatsinks. Available online: https://www.fischerelektronik.de/webfischer.com (accessed on 21 December 2021).
30. Xin, Q. *Diesel Engine System Design*, 1st ed.; Woodhead Publishing: Sawston, UK, 2011; 1088p.
31. DecoRemy, Alternators. Delco Remy 36SI™ High Output Brushless Alternator. Available online: http://www.delcoremy.com/alternators/find-by-model-family/36si (accessed on 21 December 2021).